Observation of Electron Trapping in an Intense Laser Beam

J. L. Chaloupka* and D. D. Meyerhofer*,†

Laboratory for Laser Energetics, University of Rochester, 250 East River Road, Rochester, New York 14623-1299

(Received 19 May 1999)

High-energy electrons have been trapped in an intense, single-beam, ponderomotive-optical trap. Thomson-scattered light from the center of a tightly focused pulsed laser beam is enhanced when a novel trapping focus is used. The observed spatial distribution and energy dependence of the scattered light agree with the results of computer simulations for ordinary and trapping beams.

PACS numbers: 42.50.Vk, 87.80.Cc, 94.30.Hn, 34.80.Qb

Since the discovery of the ponderomotive force over 40 years ago, it has been known that charged particles interacting with an oscillating electromagnetic field will seek regions of low intensity [1]. It was immediately proposed that with the appropriate field distribution, particles could be trapped with this force [2]. The case of electron confinement with a specially shaped laser beam has been discussed since then [3–5]. Recently we reported on the optical generation of a three-dimensional, ponderomotive-optical trap with a high-peak-power laser [6]. In this Letter we present the first evidence of electron trapping in a high-intensity laser field, with confinement of electrons with energies up to 10 keV. To our knowledge, this work represents the first controlled manipulation of electrons in a high-intensity laser field by the modulation of the spatial intensity distribution of the beam. This opens up a new direction of study in high-intensity laser-electron interactions. Here, we present the effects of trapping on linear Thomson scattering. A trapping beam could also be used to enhance the recently observed nonlinear Thomson scattering [7]. While some further experiments may use the particular geometry described in this Letter, more generally, we have shown that near-field phase control of a high-power laser beam can lead to tailored focal regions which may be optimized for a myriad of experiments.

Electrons interact with a laser field via the Lorentz force. For field distributions with a slowly varying temporal and spatial envelope, the motion of the electrons can be decomposed into a high-frequency quiver and a slower, "dark-seeking" drift [8]. The quiver motion is a direct result of the rapidly oscillating electromagnetic field, while the drift is a consequence of the ponderomotive force (the cycle-averaged Lorentz force). The ponderomotive force takes the form $\mathbf{F}_{\text{pond}} = -\nabla U_{\text{pond}}$, where $U_{\text{pond}} = (e^2 I \lambda^2)/(2\pi m c^3)$ (I is the intensity, λ is the wavelength, c is the speed of light, and e and m are the electron charge and rest mass, respectively). At low intensities, the quiver velocity is nonrelativistic and the magnetic field term in the Lorentz force can be ignored. The electron motion is a result of the electric field alone and is purely harmonic. Under these conditions, the electron undergoes linear Thomson scattering [9]. For high intensities ($I \cong 10^{18}$ W/cm^2 for $\lambda = 1$ μm light), the fully relativistic Lorentz force must be used and the electron quivers anharmonically. In this case, the electron emits harmonics of the incident field (nonlinear Thomson scattering) [7,10,11]. To reach such intensities, a short-pulse, high-energy laser beam must be focused to a small spot size. Tight focusing yields high peak intensities but also results in large intensity gradients and, therefore, large ponderomotive forces. In an ordinary centrally peaked focus, the strongest gradients point radially inward, so the ponderomotive force pushes electrons outward, directly away from the regions of high intensity.

To control the drift of electrons from the focal region, we have developed a scheme to create a focus with a local minimum at its center [6]. A uniphase laser beam, regardless of its amplitude distribution, will focus to a centrally peaked spot due to the constructive interference at the center of the focal region. By inducing a π phase shift to the central portion of an incident beam, the light from the unshifted outer region will interfere destructively with the shifted light. If half of the incident field is shifted, there will be complete destructive interference at the center of the focus, creating a field null surrounded on all sides by regions of nonzero intensity. This occurs for a π region diameter of $1.65w$ for a Gaussian beam, where w is the incident beam's $1/e^2$ (in intensity) radius [6].

Computer simulations of electron trajectories in a Gaussian focus and a trapping focus have been performed. With the trap, the electrons spend a significantly longer time interacting with the intense field. In one simulation, electrons were released into the field by barrier-suppression ionization [12] from He^{1+} at an intensity of 1.5×10^{15} W/cm^2 by a laser pulse with the same characteristics as in our laboratory [13]: $I_{\text{peak}} = 10^{18}$ W/cm^2, $w_0 = 5$ μm, $\tau = 2$ ps, and $\lambda = 1.05$ μm, where I_{peak} is the peak intensity of the ordinary beam, w_0 is the $1/e^2$ (in intensity) radius of the focal spot, τ is the FWHM pulse width, and λ is the central wavelength. The fully relativistic Lorentz force was used in this and all subsequent simulations. A typical electron released into the trapping region experiences an average intensity approximately 3 times as high for a time approximately 6 times as long as an electron released into a comparable

 0031-9007/99/83(22)/4538(4)$15.00

Gaussian focus (generated with the same near-field power distribution). These values depend on the electrons' initial location in the focal region. Similar results are obtained with different gas species and charge states. By tuning the trap minimum away from zero (by changing the size of the π region) [6], the peak intensity that the electron experiences can be increased by a factor of 10, while maintaining trapping.

The most direct signature of electron trapping is the enhanced linear Thomson scattering that results from the increased laser-electron interaction. Figure 1 shows the results of a computer code used to generate images of Thomson-scattered radiation from three different focal regions. The code uses the same laser pulse as described above and propagates electrons ionized from up to the first eight charge states in argon by barrier-suppression ionization. Since the total, time-integrated Thomson-scattered signal is a linear function of intensity, interaction time, and number of electrons, the total signal at a given point in the focal region was approximated as the sum over all times of the product of electron number, instantaneous laser intensity, and time step. Figure 1(a) shows the $w_0 = 5$ μm Gaussian focal-plane image, Fig. 1(b) shows the focal-plane image generated by a flat-top incident beam (which mimics the extra structure present in the experimental, unaltered focal spot), and Fig. 1(c) shows the focal-plane image generated by passing a flattop incident beam through an appropriately sized π phase plate. The value of the intensity walls surrounding the central minimum of the trapping beam is approximately 12% of the nontrapping beam's peak intensity. For the peak intensity achievable with this laser system, this corresponds to a wall intensity of 1.2×10^{17} W/cm^2, which is equal to a ponderomotive barrier of 12 keV.

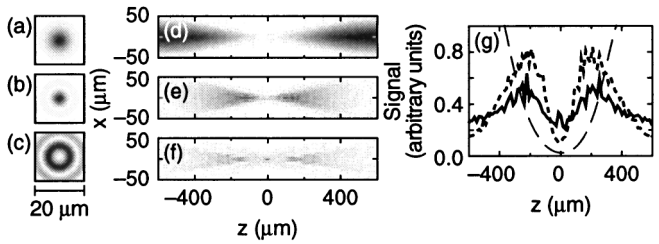

FIG. 1. Computer simulations of Thomson scattering. (a) Focal-plane image of a Gaussian beam. (b) Focal-plane image generated with a flattop incident beam. (c) Focal-plane image of a trapping beam generated with a flattop incident beam. (d) Image of the Thomson-scattered light from a Gaussian focus as viewed orthogonally to the plane of polarization. (e) Thomson-scattered image from the flattop beam. (f) Thomson-scattered image from the trapping flattop beam. (g) Total Thomson-scattered signal as a function of z (laser propagation direction) for the Gaussian beam (thin dashed line), the nontrapping flattop beam (thick dashed line), and the trapping flattop beam (solid line). The increase in signal from the center of the trapping focus is due to the confinement of electrons, while the decrease away from $z = 0$ is due to more-rapid ponderomotive expulsion along the steeper gradients in those portions of the trapping focal region.

Figure 1(d) shows the two-dimensional xz projection of the Thomson-scattered light from the Gaussian focus (the laser is polarized along the x direction and propagates along the z direction), Fig. 1(e) shows the signal from the flattop beam, and Fig. 1(f) shows the signal from the trapping flattop beam. Figure 1(g) shows the total Thomson-scattered signal for each beam type as a function of z. This corresponds to a transverse integral along x for each z position. The thin dashed line is the signal from the Gaussian focus, the thick dashed line is the signal from the nontrapping flattop focus, and the solid line is the signal from the trapping flattop focus. The signal from the regular flattop focus is substantially higher than the signal from the Gaussian focus at $z = 0$. This is due to the weak trapping that occurs in the low-intensity rings that surround the central spot. Even though the rings can capture only low-energy electrons, they represent a large volume and therefore add considerably to the total signal. At $z = 0$, the peak intensity value of the rings is 2% of the peak intensity of the central spot. A central peak intensity of 10^{18} W/cm^2 corresponds to 2-keV electrons being trapped by the rings. In contrast, the trapping focus generated with the phase plate can confine 12-keV electrons at $z = 0$. As expected, the trapping focus has the largest signal in the central focal region. Away from $z = 0$, the signal is lower than in the nontrapping case because of the more strongly peaked beam profiles of the trapping beam in those regions, resulting in more rapid ponderomotive expulsion.

To generate the trapping focus in the laboratory, a segmented wave-plate arrangement was used to induce the π-phase shift on the laser pulse [6]. A disk and annulus were cut from a half-wave plate, and the disk was rotated by 90° with respect to the annulus. In this position, the o axis of the disk coincided with the e axis of the annulus and vice versa. Since the operation of a half-wave plate relies on the retardation of a half-wave between the o and e waves, this simple arrangement adds a π phase shift to the inner portion of the beam with respect to the outer region. The size of the disk (4-cm diameter) was chosen such that approximately half of the incident field was shifted. The laser beam had an essentially flattop profile of 6.5-cm diameter, with extra energy at the center and edges of the beam.

The experimental setup for imaging Thomson-scattered radiation from the laser focus is shown in Fig. 2. The horizontally polarized (perpendicular to the plane of the figure) laser pulse enters a high-vacuum chamber from the right and is focused by an internally mounted aspherical focusing lens ($f = 20$ cm, $\phi = 12$ cm, with an 8-mm-diam block in the center). The chamber is typically backfilled with 1 to 5 Torr of nitrogen or argon. To generate the trapping beam, the wave-plate pieces are placed directly before the entrance window. The focused beam passes into and out of an aluminum tube (outer diameter of 4.4 cm) through a pair of 1.9-cm holes. The end of the tube is blocked by a solid aluminum cone that serves

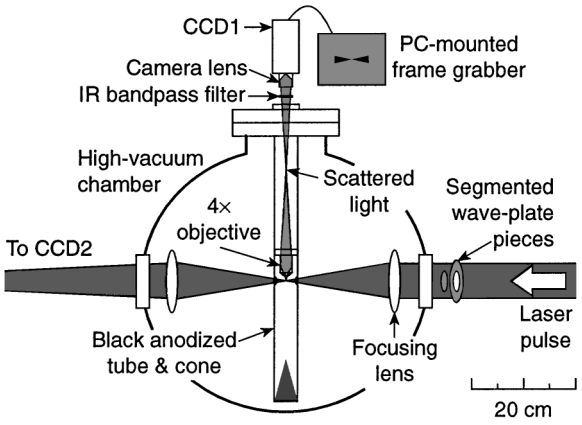

FIG. 2. Experimental arrangement for imaging Thomson-scattered light from a high-intensity laser focus. The tube and cone serve to reduce the substantial laser light background, and recombination light is eliminated by an infrared bandpass filter. The chamber is typically backfilled with a low density (1 to 5 Torr) of argon or nitrogen.

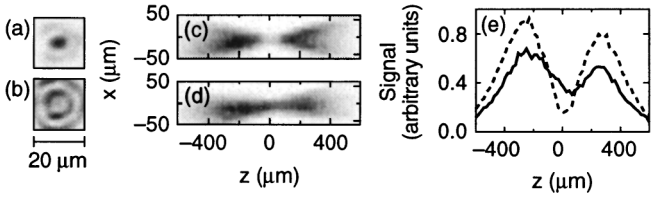

FIG. 3. Observed focal-plane images and Thomson-scattered images. (a) Ordinary beam focal-plane image taken at high power ($E = 500$ mJ) with CCD2. (b) Trapping-beam focal-plane image. (c) Image of Thomson-scattered radiation taken with CCD1 (30-laser-shot average) generated with the ordinary beam with 2.5 Torr of argon, viewed normal to the polarization direction. (d) Image generated with the trapping beam. (e) Total Thomson-scattered signal as a function of the laser propagation direction (z). The signal from the trapping beam is greater at the center of the focal region and smaller on either side, as predicted.

as a dark background for the height-adjustable 4× microscope objective. Both the tube and the cone were bead blasted and black anodized for maximum absorption of background light. The focal region is transversely imaged onto a CCD (charge-coupled device) camera (CCD1) by the objective and a camera lens (back focal length of 15 mm, open aperture of 10 mm) after passing through an infrared bandpass filter ($T_{\max} = 38\%$ at $\lambda = 1055.5$ nm, $\lambda_{\mathrm{FWHM}} = 2.5$ nm). The tip of the objective was approximately 8 mm from the laser axis. The total magnification of the imaging system (from the laser focus to the 4.8 mm × 3.6 mm CCD1 array) was 1.0. After passing through the tube, the diverging laser beam is refocused by a second lens (identical to the focusing lens) onto a second CCD camera (CCD2) approximately 6 m away (the convergence angle of the beam is exaggerated in the schematic). CCD2 was used to take images of typical focal-plane images.

The experimental results for Thomson-scattered radiation from 2.5 Torr of argon are shown in Fig. 3. Figure 3(a) shows the nontrapping focal-plane image at CCD2 (which was coupled to a 10× microscope objective for a total magnification of 150 from inside the vacuum chamber to the CCD2 array). Figure 3(b) shows the trapping focal-plane image generated with the wave-plate pieces in place. The value of the intensity walls surrounding the central minimum of the trapping beam at $z = 0$ is approximately 15% of the nontrapping beam's peak intensity, and the central minimum is less than 3% of the nontrapping beam's peak intensity. For a nontrapping beam peak intensity of 10^{18} W/cm^2, this corresponds to a trap depth at $z = 0$ of 12 keV. Away from $z = 0$, the trap wall height falls to approximately 10% of the nontrapping beam's peak intensity, giving a three-dimensional trap depth of approximately 7 keV. The focal-plane images were not noticeably affected for backfill pressures of less than 10 Torr.

Figure 3(c) shows the image of the Thomson-scattered radiation from the regular beam, and Fig. 3(d) shows the scattered image from the trapping beam. Each image is an average of 30 laser shots. The average laser energy was 500 mJ, which corresponds to a peak intensity of 7×10^{17} W/cm^2 for the nontrapping beam. The shape of the images was independent of gas species (argon or nitrogen) or pressure (1 or 2.5 Torr), and the total signal strength varied linearly with pressure. Rotating the polarization of the incident beam so it was aligned with the observation direction completely extinguished the signal, as expected for linear Thomson scattering. The total signal as a function of z [as in Fig. 1(g)] is shown in Fig. 3(e). The signal from the trapping focus is higher at $z = 0$ because of electron confinement and lower away from $z = 0$ because of steeper intensity gradients, in agreement with predictions [see Fig. 1(g)]. The asymmetry in the signal about $z = 0$ is due to the asymmetry in the intensity distribution of the laser along the propagation direction.

In addition to increased signal strength, the signal shows the expected enhanced dependence on laser intensity. In a smooth, Gaussian focus, electrons exit the focal region well before the peak of the pulse. For an electron from a given charge state released into the field at a given position, the initial intensity and spatial intensity gradient that it experiences will be the same regardless of peak intensity. As the electron leaves the laser focus, the intensity that it experiences as a function of time will be only slightly modified by the change in its temporal position in the laser pulse envelope. The total signal will, however, increase due to the increasing focal volume with intensity [14]. The effect of the increase in focal volume can be minimized by considering only the signal from the center of the focal region ($-z_0 < z < z_0$, where $z_0 = 75$ μm is the Rayleigh range of a Gaussian beam with $w_0 = 5$ μm). With the trapping focus, electrons interact with the laser pulse for a much longer period of time, therefore, the Thomson-scattered signal will be more sensitive to the peak intensity of the laser.

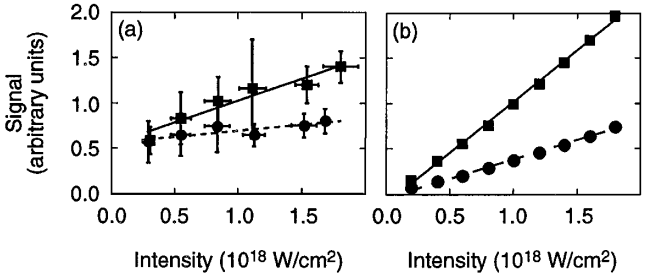

FIG. 4. Energy dependence of Thomson-scattered light from the center of the focal region. (a) Experimental results of linear Thomson scattering from several data-taking runs with the ordinary beam (circles, dashed line) and the trapping beam (squares, solid line). (b) Results from a computer simulation with an ordinary focus (circles, dashed line) and a trapping focus (squares, solid line) generated by an incident flattop beam. Both experiment and simulation show an increase in signal strength and energy dependence for the trapping beams due to the increased electron-laser interaction.

Figure 4(a) shows the experimentally measured Thomson-scattered signal from the center of the focal region as a function of laser intensity. The horizontal axis represents the peak intensity of the unaltered, nontrapping beam (laser energy could have been used equally well, where 700 mJ is equal to 10^{18} W/cm^2). The solid line is a straight-line fit to the trapping-beam signal (squares), and the dashed line is a fit to the unaltered-beam signal (circles). The gas species was either argon or nitrogen at a pressure of 1.0 or 2.5 Torr for any given run. The signal value is the total signal from the center of the focal region ($-75 < z < 75$ μm), the data from each run were normalized to the average signal strength (at $E = 700$ mJ) for each beam type, and each shot was background subtracted. The normalization of the trapping beam data was performed independently of the normalization of the nontrapping beam data. As expected, the signal strength and slope are enhanced for the trapping beam. The scatter in the data is likely due to fluctuations in the beam quality.

Figure 4(b) shows the predicted intensity scaling from the computer simulation for an ordinary focus (circles, dashed line) and a trapping focus (squares, solid line) generated from an incident flattop beam focused into argon gas. The choice of gas species is arbitrary since the overall trends are universal. As in Fig. 4(a), the signal is taken from the center of the focal region. Because of the minimal amount of trapping with the ordinary beam, the scattered signal is low and varies weakly with laser intensity. As in the experiment, the signal from the trapping beam is larger and depends more strongly on laser energy. The calculated contrast in signal strength and slope between ordinary and trapping beams is even greater when using a perfect Gaussian incident beam. A greater calculated signal enhancement is observed when using a "bright" trap, whose trapping region has a nonzero intensity minimum [6]. In such a trap, the effect on the nonlinear Thomson-scattered signal is especially pronounced since electrons are confined in a region of high field. Simulations show that for an unaltered beam's peak intensity of $I_0 = 10^{19}$ W/cm^2, the nonlinear signal from the center of a bright trap ($I_{\text{center}} = 0.20 I_0$) is 2.2×10^4 times larger than the signal from the center of a Gaussian focus.

In conclusion, we have made the first observation of electron trapping in an intense laser beam. A novel segmented wave-plate scheme was used to generate the trapping focus. Electron trapping in the altered focus resulted in enhanced linear Thomson scattering from the center of the focal region as predicted by computer simulations. The observed increase in energy dependence was also expected. Computer simulations show that the trapping focus would also increase the signal generated by nonlinear Thomson scattering.

The authors thank A. Maltsev for machining the $\lambda/2$ plate. We also thank N. P. Bigelow, J. H. Eberly, Y. Fisher, and T. J. Kessler for helpful discussions. This research was supported by the National Science Foundation, with additional support by the U.S. Department of Energy Office of Inertial Confinement Fusion under Cooperative Agreement No. DE-FC03-92SF19460, the University of Rochester, and the New York State Energy Research and Development Authority. The support of the DOE does not constitute an endorsement by the DOE of the views expressed in this Letter.

*Also at Department of Physics and Astronomy.
†Also at Department of Mechanical Engineering.

[1] H. A. H. Boot and R. B. R.-S. Harvie, Nature (London) **180**, 1187 (1957).
[2] V. Gapanov and M. A. Miller, J. Exp. Theor. Phys. (USSR) **34**, 242 (1958).
[3] N. J. Phillips and J. J. Sanderson, Phys. Lett. **21**, 533 (1966).
[4] U. Mohideen, H. W. K. Tom, R. R. Freeman, J. Bokor, and P. H. Bucksbaum, J. Opt. Soc. Am. B **9**, 2190 (1992).
[5] C. I. Moore, J. Mod. Opt. **39**, 2171 (1992).
[6] J. L. Chaloupka, Y. Fisher, T. J. Kessler, and D. D. Meyerhofer, Opt. Lett. **22**, 1021 (1997).
[7] S.-Y. Chen, A. Maksimchuk, and D. Umstadter, Nature (London) **396**, 653 (1998).
[8] J. H. Eberly, in *Progress in Optics*, edited by E. Wolf (North-Holland, Amsterdam, 1969), Vol. 7.
[9] J. D. Jackson, *Classical Electrodynamics* (Wiley, New York, 1975), 2nd ed.
[10] Vachaspati, Phys. Rev. **128**, 664 (1962).
[11] E. S. Sarachik and G. T. Schappert, Phys. Rev. D **1**, 2738 (1970).
[12] S. Augst, D. D. Meyerhofer, D. Strickland, and S. L. Chin, J. Opt. Soc. Am. B **8**, 858 (1991).
[13] Y.-H. Chuang, D. D. Meyerhofer, S. Augst, H. Chen, J. Peatross, and S. Uchida, J. Opt. Soc. Am. B **8**, 1226 (1991).
[14] M. D. Perry, O. L. Landen, A. Szöke, and E. M. Campbell, Phys. Rev. A **37**, 747 (1988).